Atom-economic enantioselective photoenzymatic radical hydroalkylation via single-electron oxidation of carbanions

Jin Zhu[1,2,6], Qiaoyu Zhang[3,6], Tao Gu[2,6], Binbin Chen[2], Mingzhe Ma[2], Xiaoyu Wang[3], Xiao Liu[2], Mingjie Ma[2], Binju Wang[3*], and Yajie Wang[2,4,5*]

[1]School of Materials Science and Engineering, Zhejiang University, Hangzhou, Zhejiang 310058, China.

[2]School of Engineering, Westlake University, Hangzhou 310030, China.

[3]Key Laboratory of Theoretical and Computational Chemistry, College of Chemistry and Chemical Engineering, Xiamen University, Xiamen 361005, China.

[4]School of Life Science, Westlake University, Hangzhou 310030, China.

[5]Westlake Center of Synthetic Biology and Integrated Bioengineering, Westlake University, Hangzhou 310030, China.

[6]These authors contributed equally: Jin Zhu, Qiaoyu Zhang, and Tao Gu.

*Corresponding author Emails: wangbinju2018@xmu.edu.cn; wangyajie@westlake.edu.cn

Abstract

Established strategies for enantioselective hydroalkylation for C(sp^3)–C(sp^3) bond formation usually require pre-functionalized substrates as radical precursors in both transition-metal and photoenzymatic catalysis. Based on a sequential proton transfer/electron transfer (PT/ET) strategy, here we show a cooperative photoenzymatic system consisting of a flavin-dependent 'ene'-reductase (ER) and an organophotoredox catalyst fluorescein (FI) to achieve atom-economic enantiodivergent hydroalkylation of electron-deficient C(sp^3)–H with olefins. Mechanistic studies revealed a pathway for radical intermediate formation via excited-state FI^*-induced single-electron oxidation of carbanions under alkaline conditions. The overall catalytic efficiency is enhanced by the electron transfer (ET) between FMN_{ox} and $FI^{\bullet-}$, while the stereoselectivity is controlled by ERs through enantioselective hydrogen atom transfer (HAT). We anticipate that this mode of photoenzymatic catalysis will inspire new pathways for generating free radical intermediates and foster innovative strategies for achieving photoenzymatic new-to-nature reactions.

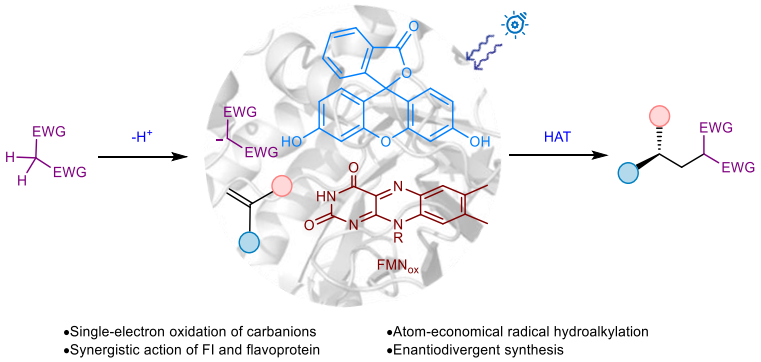

Introduction

The formation of C(sp^3)–C(sp^3) bonds presents a significant synthetic challenge but is crucial in synthetic chemistry due to their fundamental role in constructing the carbon backbone of organic molecules[1-3]. Traditional chemocatalytic approaches include S_N2-type substitution reactions of enolates with alkyl halides[4,5] and transition metal-catalyzed cross-couplings[6,7]. The former strategy often requires strong bases and lacks monoalkylation control, while the latter is limited by β-hydrogen elimination in alkyl-metal species[1,2]. In contrast, radical hydroalkylation of cost-effective, readily available olefins has become an important strategy[8,9]. Common methods include single-electron reduction of halides[10-13], proton-coupled electron transfer of diazo compounds[14], and redox decarboxylation of carboxylic acids[15-17] or esters[18-20]. However, these methods often require pre-functionalized substrates as radical precursors, impacting atom economy and necessitating pre-synthesis. While transition metal catalysis typically achieves enantioselectivity through metal hydride migratory insertion into olefins or radical trapping[12,21], it struggles with remote stereocontrol at sites distant from the chiral environment[22,23]. State-of-the-art catalysis prioritizes maximum efficiency and sustainability through stringent adherence to step and atom economy, mild conditions, coupled with precise stereochemical control[24-26], thus posing challenges for enantioselective radical hydroalkylation.

Recent advancements in photoenzymatic catalysis have shown remarkable enantioselectivity in the asymmetric hydrogen atom transfer (HAT) of prochiral radicals[27-39], especially in remote stereocontrol[29,30]. Radicals are generated either

through the single-electron reduction of an electron-donor-acceptor (EDA) complex (Fig. 1a and 1b)[27-34] or via the single-electron oxidation of electron-rich precursors[35-39]. These methods have been successfully developed for selective hydroalkylation of halides[27-32], NHPI esters[33], diazo compounds[34], and carboxylic acids[35] with olefins, also largely relying on pre-functionalized substrates. In contrast, generating radicals through the homolytic cleavage of C–H bonds (Fig. 1c) in single-electron oxidation-initiated photoenzymatic catalysis shows excellent atom economy[36,37]. However, this approach has been restricted to the functionalization of electron-rich olefins and aromatics for lactonization[36] and hydroarylation[37]. Therefore, developing atom-economic enantioselective hydroalkylation is of great scientific importance in both fields of transition metal catalysis and photoenzymatic catalysis.

Given the critical role of cyano, carbonyl, and ester groups in late-stage functionalization[40], the hydroalkylation of olefins with precursors containing these electron-withdrawing groups (EWG) is essential. Thus, electron-deficient C(sp^3)–H bonds, activated by the adjacent EWGs, can serve as effective radical precursors for atom-economic hydroalkylation process. Although highly electron-deficient alkanes resist oxidation, they can be readily deprotonated to yield carbanions. Building on advances in synthetic chemistry, protic C(sp^3)–H bonds can undergo radical activation through multiple pathways, including proton-coupled electron transfer (PCET), sequential PT/ET, and ET/PT[41]. This prompted our investigation of a PT/ET strategy, where electron-deficient substrates form carbanions via deprotonation, followed by single-electron oxidation to generate radical intermediates. Building on this hypothesis,

we developed a cooperative photoenzymatic system comprising an ene-reductase (ER) and an organophotoredox fluorescein to achieve the enantioselective radical hydroalkylation of electron-deficient C(sp^3)–H bonds with olefins. In this catalytic process, carbanions are generated under alkaline conditions and oxidized to radicals through an excited-state photocatalyst-induced single-electron transfer (SET). Stereoselectivity is achieved via an enantioselective HAT step of prochiral intermediates mediated by ER (Fig. 1d). This photoenzymatic system reveals a mechanism for radical formation that is rarely reported in photoredox catalysis, enabling an atom-economic and enantioselective radical hydroalkylation process.

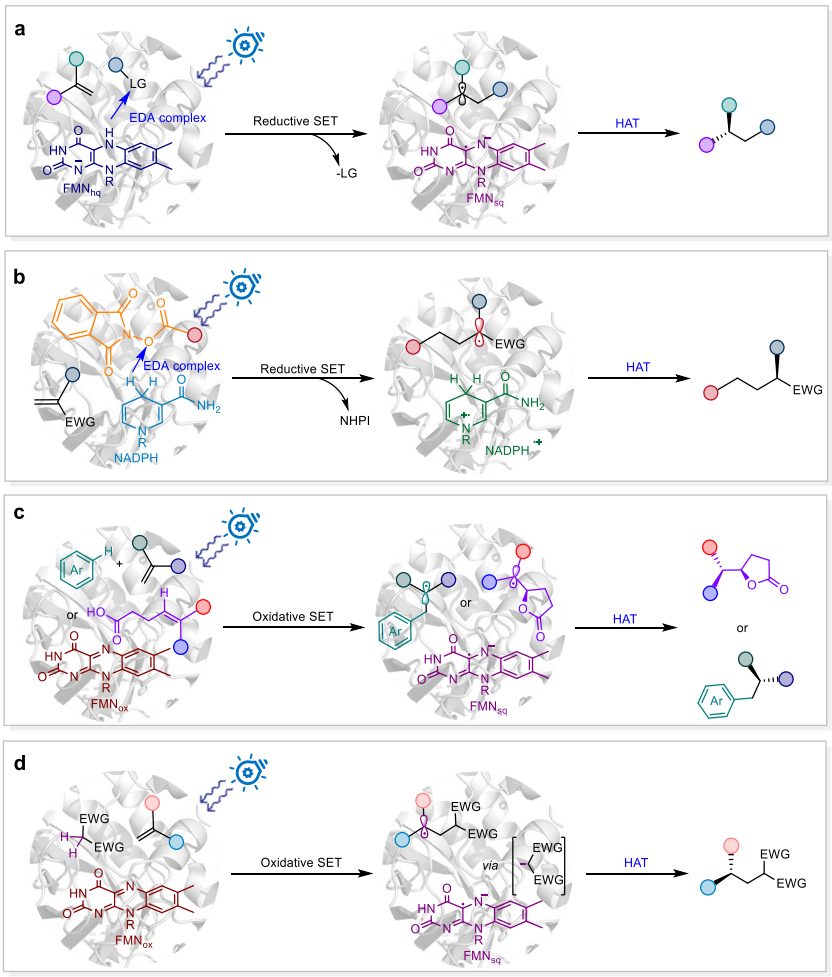

Fig. 1| Different photoenzymatic modes for enantioselective hydrofunctionalization.

87 **Results and Discussion**

88 **Reaction development and engineering**

89 While photoredox catalysis has successfully generated radicals from carbanions via
90 single-electron oxidation[41-43], this reactivity remains unexplored in biocatalysis systems.
91 The key challenge lies in the high reactivity of carbanions, complicating control over
92 single-electron oxidation versus competing pathways such as nucleophilic addition to
93 electrophilic π-systems[44,45]. Highly electrophilic radicals can also quickly convert into
94 carbanions through reductive radical polar crossover (RRPCO)[46,47]. To develop a
95 photoenzymatic system for the enantioselective radical hydroalkylation of electron-
96 deficient C(sp^3)–H bonds with olefins, suitable enzymes must remain active in alkaline
97 conditions necessary for carbanion formation. The excited ER-FMN_{ox}^* must effectively
98 oxidize carbanions into free radicals while minimizing undesirable pathways, such as
99 carbanion nucleophilic addition, reductive quenching of FMN_{ox}^* by the reaction buffer
100 or nearby amino acids, and RRPCO (Supplementary Fig. 9).

101 We investigated the proposed reactions using malononitrile **1a** and α-methylstyrene
102 **2a** as model substrates with a library of ERs at 1 mol% under 455 nm blue LED
103 illumination. Most ERs showed no catalytic activity (Table 1, entry 1 and
104 Supplementary Table 3), but MorB, OYE2, SYE1, SYE2, SYE3, and GluER achieved
105 yields of 1.2% to 3%. Notably, SYE2 and GluER exhibited the best and opposite
106 enantioselectivity for **3a**. GluER had (*S*)-selectivity with a 4:96 enantiomeric ratio (er)
107 (Table 1, entry 2), while SYE2 showed (*R*)-selectivity with a 93.3:6.6 er (Table 1, entry
108 3). Thus, SYE2 and GluER were chosen for further investigation.

To enhance the yield of **3a**, we tested various reaction conditions, including buffer systems, pH levels, and co-solvents (Supplementary Tables 4-5). Although these adjustments did not significantly improve the yield, we decided to proceed with Tris buffer at pH 9 and ethanol as a co-solvent. Notably, the reaction only occurs at pH 9 or above, indicating that strongly alkaline conditions are essential for initiating carbanion formation in the catalytic cycle (Table 1, entries 4-6).

Unlike other photoenzymatic systems[37,38], adding extra FMN-Na did not enhance the yield of **3a** (Table 1, entry 7). This suggests that FMN_{ox}^{*}-induced single-electron oxidation of carbanions may be the rate-limiting step, indicating the need for photocatalysts with higher oxidative potential. We screened 18 transition metal and organic photocatalysts (Supplementary Tables 6-7) and identified fluorescein (FI-PC7), PC9, and PC12 as effective, increasing the yield of **3a** to 27%, 21%, and 19%, respectively, in both SYE2 and GluER-catalyzed reactions. The combination of 5 mol% FI with 1 mol% SYE2 or GluER gave the highest yields of **3a**, at 47.8% and 45.5%, respectively, without compromising enantioselectivity (Table 1, entries 8-9). Control experiments without light or in the presence of air did not produce the target product (Table 1, entries 10-11), supporting the visible-light-induced radical mechanism. Although neither FMN nor FI alone could catalyze the transformation (Table 1, entries 12-13), combining 10 mol% of both resulted in a 3% racemate of **3a** (Table 1, entry 14). These findings indicate that FI and FMN cooperate to catalyze the C(sp^3)-H functionalization process, highlighting the essential role of photoenzymes in improving efficiency and controlling the stereochemistry of radical processes.

131 **Table 1 | Optimization of reaction conditions for photoenzymatic enantioselective**

132 **C(sp^3)-H functionalization.**

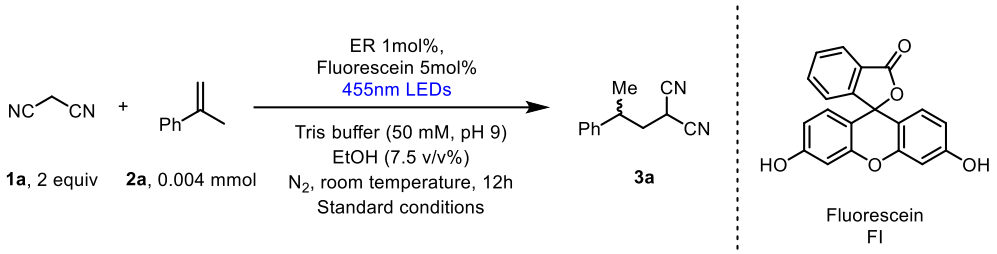

133

Entry	ER	Deviation from standard conditions[a]	Yield (%)[b]	er (%) (R:S)[c]
1	ERs[d]	w/o FI	n.r.	n.a.
2	GluER	w/o FI	1.3	4:96
3	SYE2	w/o FI	2.6	93.3:6.6
4	SYE2	Tris buffer pH 7.4, w/o FI	n.r.	n.a.
5	SYE2	Tris buffer pH 8, w/o FI	n.r.	n.a.
6	SYE2	Tris buffer pH 10, w/o FI	1.5	85:13
7	SYE2	w/o FI, 10 mol% FMN-Na	2.6	93.3:6.6
8	**SYE2**	**None**	**47.8**	**95.6:4.4**
9	**GluER**	**None**	**45.5**	**1.2:98.8**
10	SYE2	Dark	n.r.	n.a.
11	SYE2	Air	n.r.	n.a.
12	/	FMN-Na instead FI	n.r.	n.a.
13	/	None	n.r.	n.a.
14	/	10 mol% FMN-Na + FI	3	racemate

134 [a]Conditions: the total volume of standard reaction was 400 uL. [b]Yield was determined by gas
135 chromatography. c er was determined by HPLC analysis on a chiral stationary phase, and the
136 absolute configuration was established by theoretical calculations of electronic circular
137 dichroism (ECD); see Supplementary Fig. 31 and Fig. 32. [d]LacER, KYE1, OYE1, OYE3, OPR1,
138 SYE4, TOYE and YqjM were tested. n.r. No reaction; n.a. Not applicable.

139

140 **Substrate scope investigations**

141 We explored the substrate scope using SYE2 (ER1) and GluER to access both

142 enantiomers of the products. While both enzymes showed excellent enantioselectivity

143 for **3a**, this decreased significantly for most derivatives (Supplementary Fig. 33). To
144 address this, we engineered GluER using site-saturated mutagenesis. Molecular
145 docking of GluER's crystal structure with **1a** and **2a** identified key residues in the
146 substrate channel and FMN binding region, including T36, W66, H172, N175, Y177,
147 T231, Q232, P239, R261, F269, and Y343 (see Supplementary Fig. 2). Site-saturated
148 mutagenesis of these 11 sites led to GluER-Y343A (ER2), which showed improved
149 enantioselectivity for both **3a** (up to R:S = 99.5:0.5) and other derivatives (Fig. 2).

150 The photoenzymatic system enabled hydroalkylation of various substituted methyl
151 styrenes with functional groups at the para-/meta-/ortho positions of the phenyl group
152 (**3a-j**), producing stereodivergent products with moderate to good yields and up
153 to >1:99 er. Although 1-bromo-2-(prop-1-en-2-yl)benzene (**3k**) had a relatively low
154 yield, it exhibited good to excellent enantioselectivity. Additionally, 2-naphthyl (**3l**),
155 benzothiophene (**3m**), and biphenyl (**3n**) demonstrated the compatibility of
156 photoenzymatic catalysis with aromatic rings and heterocycle. Variations at the α
157 position of styrene had minimal impact on outcomes, as seen with **3p**. However,
158 replacing aromatic olefins with aliphatic olefins significantly reduced the yield of **3o**.
159 Although the mutant GluER-W66Q-Y343A (ER3) improved the yield of **3o**, the
160 enantioselectivity remained unsatisfactory. Beyond malononitrile **2a**, dimethyl
161 malonate **2b** could also alkylate with **3q** with excellent enantioselectivity. Moreover,
162 this photoenzymatic catalysis can be successfully scaled up to 1 mmol with minimal
163 changes in yield and enantioselectivity.

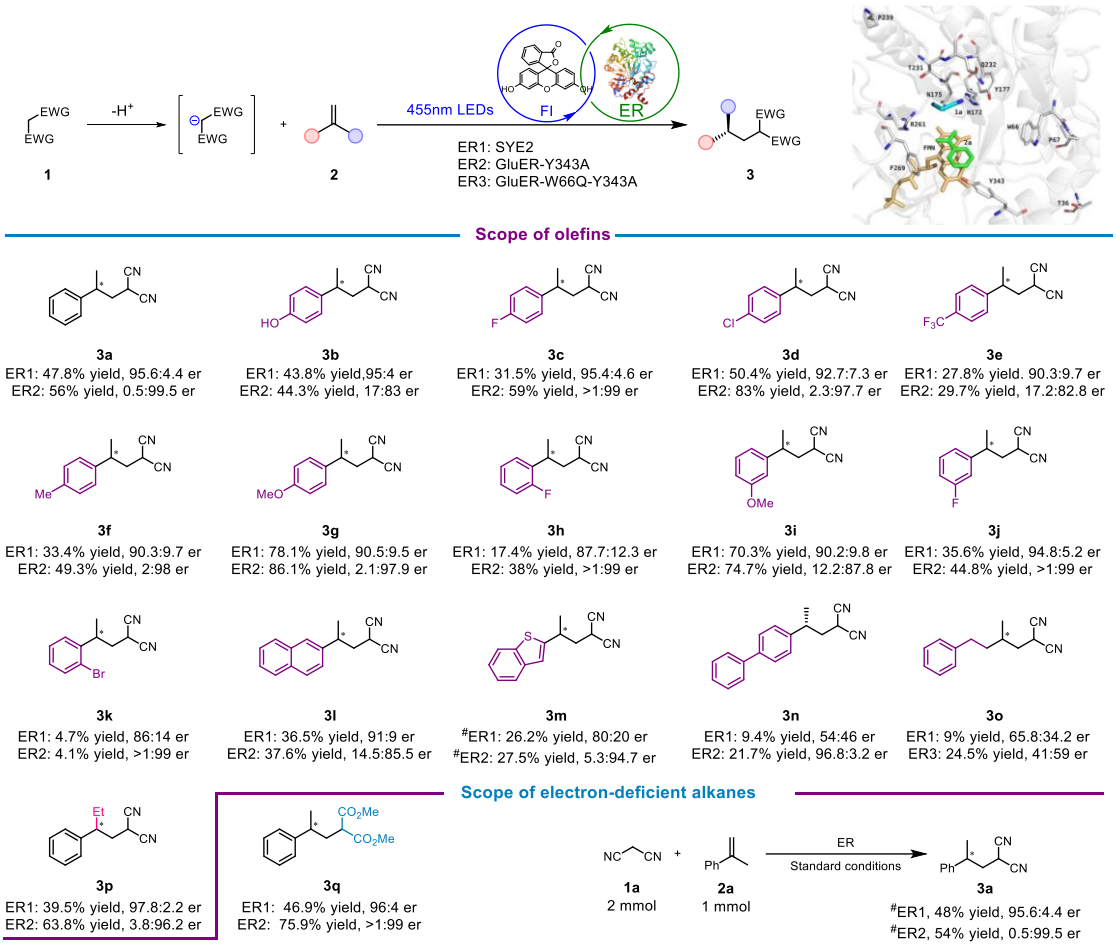

Fig. 2 | Substrate scope of enantioselective functionalization of electron-deficient C(*sp*^{3})-H bonds via hydroalkylation catalyzed by cooperative photoenzymatic system. Conditions: 1 (0.008 mmol), 2 (0.004 mmol), ER (1 mol%), FI (5 mol%), and EtOH (7.5 v/v%) in Tris buffer (50 mM, pH 9) were stirred at room temperature for 12 hours under N_2 with 455 nm LEDs. The total reaction volume was 400 μL. Yields were determined by gas chromatography, and the er by HPLC on a chiral stationary phase. # Isolated yield was obtained by scaling up the reaction.

Mechanistic investigations

Based on the experimental results, we proposed a synergistic photoredox and biocatalytic mechanism for new-to-nature photoenzymatic C(*sp*^{3})-H functionalization (Fig. 3a and detailed in Supplementary Fig. 22). In this catalytic cycle, malononitrile **1a** is first deprotonated in alkaline solutions to form carbanion intermediate **Int. A**. The

178 light-excited photocatalyst FI^* then oxidizes **Int. A** via SET, producing malononitrile
179 free radical **Int. B** and fluorescein radical anion $FI^{-\bullet}$. **Int. B** subsequently attacks α-
180 methylstyrene **2a**, forming a C-C bond and generating prochiral radical intermediate
181 **Int. C**, alongside FMN_{sq} from FMN_{ox} capturing an electron from $FI^{-\bullet}$. Finally, **Int. C**
182 undergoes ER-mediated enantioselective HAT, yielding enantioenriched **3a**, while
183 $FMNH^{\bullet}$ is oxidized back to FMN_{ox}, completing the catalytic cycle.

184 Several experiments were performed to support the proposed mechanism. The
185 photophysical properties of SYE2 and FI were measured to identify visible-light-
186 excited species. UV-vis absorption spectra show that SYE2 and FI absorb in the ranges
187 of 400-520 nm and 420-530 nm, with maximum absorptions at 460 nm and 490 nm,
188 respectively (Fig. 3b). This confirms that FI can be effectively excited by 455nm LED
189 to initiate the catalytic cycle. Stern-Volmer luminescence quenching experiments also
190 support the initial reductive quenching of excited FI^* by **1a** (**Int. A** → **Int. B**), as the
191 fluorescence intensity of FI decreased upon adding **1a**, unlike with **2a** (Supplementary
192 Fig. 10).

193 Several experiments were also performed to verify the generated radical
194 intermediates. Firstly, the radical trapping experiment was performed by adding 2
195 equivalents of 2,2,6,6-tetramethylpiperidine-1-oxyl (TEMPO) to the reaction mixture
196 under standard conditions. Only trace amounts of **3a** were detected, as the prochiral
197 radical intermediate **Int. C** was trapped by TEMPO, confirmed by high-resolution mass
198 spectrometry (HRMS) (Fig. 3c). Additionally, when α-cyclopropyl styrene **4** was
199 subjected to the photoenzymatic system, the ring-opening product **5** was observed as

200 the major product, supporting the involvement of **Int. C** (Fig. 3d). To further investigate
201 the photo-oxidation step and clarify the resulting radical intermediates, electron
202 paramagnetic resonance (EPR) experiments were conducted. With 5,5-dimethyl-1-
203 pyrroline *N*-oxide (DMPO) as a radical trapping agent, slight changes in EPR signals
204 were observed in the presence of **1a** compared to **2a** (Fig. 3b), indicating the formation
205 of a potential **1a**-derived radical (**Int. B**), consistent with quenching experiments. The
206 difference in EPR signals with and without **2a** suggests that the malononitrile radical
207 **Int. B**, generated from the single-electron oxidation of the unstable carbanion **Int. A**,
208 rapidly reacts with **2a** to form a more stable prochiral benzyl radical **Int. C** before being
209 captured.[45]

210 Since apo-SYE2 (SYE2 without FMN) and FI alone did not catalyze the product
211 formation, and adding extra FMN restored reactivity, we confirmed that the catalytic
212 cycle requires the cooperative action of ER_FMN and FI (Fig. 3e and detailed in
213 Supplementary Table 8 and Fig. 17). Finaly, deuterium-labelling experiments were
214 conducted to investigate the final termination step (Fig. 3f). Using a deuterated buffer,
215 the hydrogen at the stereogenic center was labelled at 76% D, suggesting that water
216 may be involved in HAT steps.

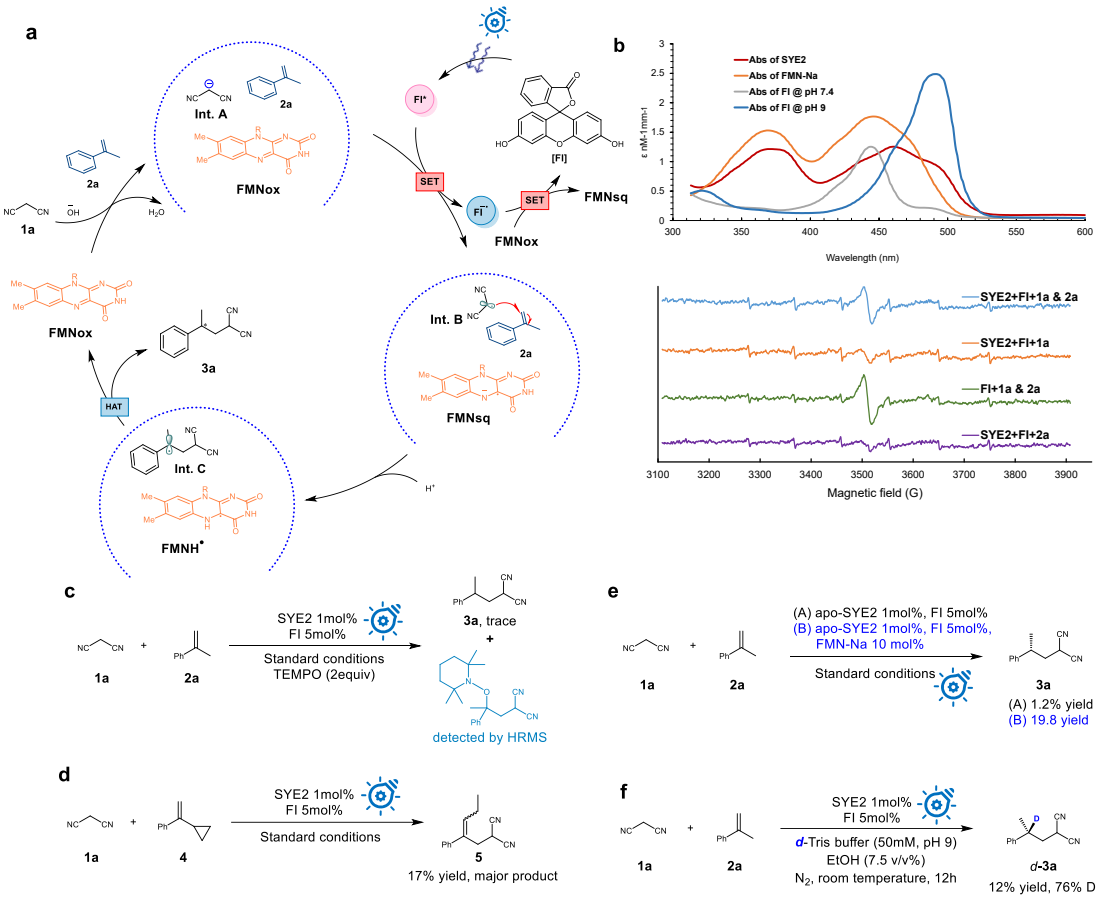

Fig. 3 | Mechanistic experiments and proposed catalytic cycle. a, Proposed catalytic cycle. **b**, UV-vis absorption (abs) spectra and room-temperature EPR experiments. **c**, TEMPO trapping experiment. **d**, Radical clock experiment. **e**, Photoenzymatic reactions catalysed by apo-flavoprotein. **f**, Deuterium-labelling experiment.

Computational studies

Extensive computational studies were performed to rationalize the mechanism proposed in Fig. 3a. Using hybrid cluster-continuum (HCC) model calculations, we found that **1a** undergoes facile deprotonation by OH^- ions in aqueous solution, forming the anionic species **Int. A.** with a low energy barrier of 0.3 kcal/mol (Supplementary Figure 20). To ascertain that **Int. A**, rather than **1a**, serves as the reactant for the generation of the carbanion intermediates **Int. B**, density functional theory (DFT)

230 calculations and time-dependent DFT (TD-DFT) calculations were conducted. The
231 Gibbs reaction energy (ΔG) for the excited FI^*-mediated oxidation of **1a** and **Int. A**
232 were calculated to be +105.2 kcal/mol and -32.1 kcal/mol (Fig. 4a and Supplementary
233 Fig. 15), respectively, supporting that photoinduced single-electron oxidation process
234 occurs through carbanion intermediates **Int. A**.

235 Since EPR experiments with FI, **1a**, and **2a** revealed distinctive radical signals,
236 suggesting that the formation of **Int. C** might be independent on ER participation.
237 Quantum mechanics (QM) model calculations show that the radical addition between
238 **Int. B** and **2a** has an energy barrier of 3.0 kcal/mol and an exothermicity of 10.7
239 kcal/mol (Fig. 4b), suggesting that formation of **Int. C** is quite facile. In addition,
240 deuteration experiments and the pKa value of FMN_{sq} (~8.5) suggested that the
241 protonation of FMN_{sq} to form neutral $FMNH^{\bullet}$ is feasible at pH 9, with a Gibbs reaction
242 energy (ΔG) of ~0.7 kcal/mol. Starting from $FMNH^{\bullet}$, HAT from $FMNH^{\bullet}$ to **Int. C** is
243 expected to yield the final product **3a**.

244 To elucidate the opposing enantioselectivity of GluER and SYE2, **Int. C** and FI
245 were docked into the enzyme active sites. Molecular dynamics (MD) simulations
246 indicate that FI was stabilized by Arg261 in GluER (Supplementary Fig. 23). **Int. C**
247 adopts two distinct conformations (CH_3-left and CH_3-right) in GluER, corresponding
248 to the *R* and *S* configurations, respectively. Moreover, the quantum mechanics
249 /molecular mechanics (QM/MM)-calculated HAT barriers are 16.2 kcal/mol for the
250 CH_3-right and 23.2 kcal/mol for the CH_3-left, aligning with the observed dominant
251 product (*S*)-**3a** (Fig. 4c and Fig. 4d). This is likely due to steric repulsion between the

252 bulky-CN substituent of **Int. C** and $FMNH^{\bullet}$ in the CH_3-left conformation, which tends
253 to enlarge the distance between the C3 atom of **Int. C** and the N5-H of $FMNH^{\bullet}$ (4.10 Å
254 in CH_3-left vs. 3.44 Å in CH_3-right), thereby increasing the energy barrier for HAT in
255 CH_3-left conformation.

256 Unlike GluER, MD simulations reveal that the bulky-CN substituents in the CH_3-
257 left conformation of **Int. C** forms a stable hydrogen bond with Tyr180 in SYE2, which
258 positions bulky-CN away from $FMNH^{\bullet}$ and facilitates the subsequent HAT process, that
259 is favor of generating (*R*)-**3a** (Supplementary Fig. 26). Indeed, our calculations suggest
260 that the HAT process in SYE2 involves a barrier of 17.2 kcal/mol in the CH_3-left
261 conformation and 22.0 kcal/mol in the CH_3-right conformation, leading to the dominant
262 formation of (*R*)-**3a** that agrees with experiments (Supplementary Fig. 26 and Fig. 27).

263 Furthermore, the newly formed $FI^{-\bullet}$ could reduce FMN_{ox} to FMN_{sq} and release the
264 initial ground state FI. DFT calculations show that $FI^{-\bullet}$ has the lowest redox potential
265 among all functional photocatalysts (PC1, PC2, PC5, FI, PC10, and PC12), making it
266 highly prone to transfer an electron to FMN_{ox} to form FMN_{sq} (Supplementary Fig. 16).
267 This suggests that ET between FMN_{ox} and $FI^{-\bullet}$ enhances the whole catalytic process,
268 explaining why FI is the most effective among all tested photocatalysts.

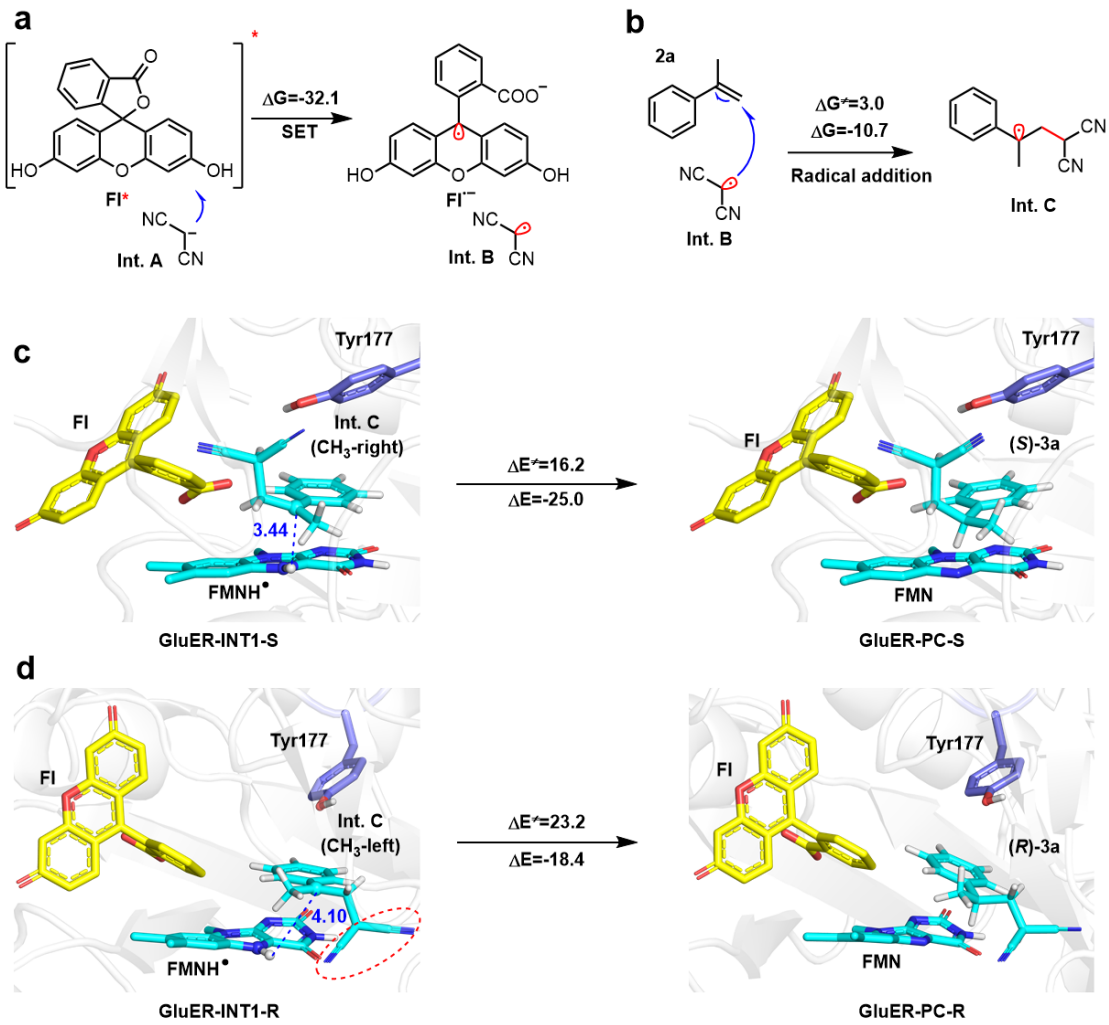

Fig. 4 | Mechanistic studies. a. SET from the excited FI* to **Int. A**. **b**, The radical addition reaction between **Int. B** and **2a. c**, QM/MM-calculated energy of the HAT process from FMNH• to the **Int. C** (CH_3-right) result in the production of *S*-(**3a**). **d**, QM/MM-calculated energy of the HAT process from FMNH• to the **Int. C** (CH_3-left) result in the production of *R*-(**3a**).

Conclusions

In summary, we have developed a synergistic photoenzymatic system for the enantioselective functionalization of electron-deficient C(sp^3)-H bonds through radical intermediates generated by photoinduced single-electron oxidation of carbanions. This

280 enantiodivergent strategy, demonstrated in 17 cases with enantiomeric ratios up
281 to >1:99 and yields of up to 83%, offers potential for the one-step construction of
282 dicyano and diester compounds with remote stereocenters. Detailed mechanistic
283 experiments confirmed that the excited-state photocatalyst FI^* performs single-electron
284 oxidation of carbanion rather than directly oxidizing the electron-deficient
285 malononitrile **1a** to generate free radical intermediates. Unlike previous
286 photoenzymatic systems, the ET between the additional photocatalyst FI and FMN_{ox}
287 ensures catalytic cycle's smooth operation. This novel mode of photoenzymatic
288 catalysis is expected to inspire new strategies for forming free radical intermediates and
289 enabling new-to-nature biotransformation.
290

291 **Methods**

292 **General procedure for photoenzymatic reactions**

293 Taking **1a** + **2a** → **3a** as an example, in a glovebox (O_2 concentration <5 ppm), ,
294 solutions of ene-reductase (1 mol%), FI (10 μL, 2 mM stock in EtOH, 5 mol%), and
295 substrates mix (20 μL, 400 mM **1a** and 200 mM **2a** in EtOH) were added to a 4 mL vial
296 containing a magnetic stir bar and Tris buffer (50 mM, pH 9). The total volume of the
297 reaction mixture was 400 μL and the final concentrations for EtOH was 7.5%. The vial
298 was sealed with a screw cap, removed from the glove box, illuminated with blue LEDs,
299 and stirred for 12 h with a cooling fan (see Supplementary Fig. 3 for reaction setup).
300 For the reaction where the yield was determined by gas chromatography (GC), EtOAc
301 (1.0 mL) and 10.0 μL of an internal standard stock (20 mg/mL of n-dodecane in EtOAc)

302 were added to the reaction mixture and mixed thoroughly. For the reaction where the
303 yield was determined by reverse phase HPLC, MeCN (1.0 mL) and 10.0 μL of an
304 internal standard stock (16.8 mg/mL of 1,3,5-trimethoxybenzene in MeCN) were added
305 to the reaction mixture and mixed thoroughly. The organic phase was separated and
306 then analyzed by GC (or reverse phase HPLC), GC-MS and chiral HPLC. Product
307 formation was confirmed by comparing retention times in GC/HPLC, as well as mass
308 spectra and ^{1}H-NMR spectra of the crude material with those of the reference. Yield
309 determined by GC was relative to the n-dodecane internal standard, while yield
310 determined by reverse phase HPLC was relative to the 1,3,5-trimethoxybenzene
311 internal standard. Enantioselectivity was determined by chiral HPLC.
312

313 **System setup and MD simulations**

314 The initial wild-type structure of GluER, was constructed based on the crystal structure
315 (PDB code: 6O08). The SYE2 enzyme structure was modeled using AlphaFold2, and
316 the position of FMN was confirmed by superimposing it with the GluER enzyme. Then,
317 the **Int. C** and FI were docked into the active sites using AutoDock Vina tool. 100 ns
318 MD simulations under the NPT ensemble. All MD simulations were performed with
319 GPU version of Amber 18 package.
320

321 **QM/MM calculations for enzymatic reactions**

322 A representative snapshot extracted from the clustering results in the MD trajectory was
323 used for subsequent QM/MM calculations. All QM/MM calculations were performed

using ChemShell combining Turbomole for the QM region and DL_POLY for the MM region. The electronic embedding scheme was used to account for the polarizing effect of the enzyme environment on the QM region.In all QM/MM geometry optimizations, the QM region was treated with the B3LYP functional using the double-zeta basis set def2-SVP for all atoms (labeled as B1). The energies were further corrected with the larger basis set def2-TZVP for all atoms (labeled as B2). Grimme's D3BJ empirical dispersion was included in all calculations.

DFT Calculations

All DFT calculations were performed with the Gaussian 16, Revision A.03 software. The initial structures were first optimized in conjunction with the SMD continuum solvation model at the B3LYP-D3/6-31G(d) level of theory. The solvation energies were further calculated at the M052X/6-31G* for all atoms. In particular, the solvent of water was used to simulate the reaction system.

TDDFT Calculations

The initial structures were first optimized at B3LYP/6-31G(d) level. Then, the single-point TDDFT calculations at wB97XD/6-311+G(d,p) levels were performed to compute the three low-lying singlet excited states. All TDDFT calculations were performed with Gaussian 16, Revision A.03.

Reporting summary

Further information on research design is available in the Nature Portfolio Reporting Summary linked to this article.

Data availability

Data relating to the materials and methods, experimental procedures, mechanistic studies and computational calculations, HPLC spectra, and NMR spectra are available in the Supplementary Information or from the authors on reasonable request. The atomic coordinates of the optimized computational models are available in the Supplementary Data.

References

1. Wang, J. Z., Lyon, W. L & MacMillan, D. W. C. Alkene dialkylation by triple radical sorting. *Nature* **628**, 104-109 (2024).

2. Choi, J. & Fu, G. C. Transition metal-catalyzed alkyl-alkyl bond formation: another dimension in cross-coupling chemistry. *Science* **356**, eaaf7230 (2017).

3. Zetzsche, L. E. & Narayan, A. R. H. Broadening the scope of biocatalytic C–C bond formation. *Nat. Rev. Chem.* **4**, 334-346 (2020).

4. Denes, F., Perez-Luna, A. & Chemla, F. Addition of metal enolate derivatives to unactivated carbon–carbon multiple bonds. *Chem. Rev.* **110**, 2366-2447 (2010).

5. Yamashita, Y., Ogasawara, Y., Banik, T. & Kobayashi, S. Photoinduced efficient catalytic α-alkylation reactions of active methylene and methine compounds with nonactivated alkenes. *J. Am. Chem. Soc.* **145**, 23160-23166 (2023).

6. Kranthikumar, R. Recent advances in C(sp^3)–C(sp^3) cross-coupling chemistry: a dominant performance of nickel catalysts. *Organometallics* **41**, 667-679 (2022).

7. Le, C., Liang, Y., Evans, R. W., Li, X. & MacMillan, D. W. C. Selective sp^3 C–H alkylation via polarity-match-based cross-coupling. *Nature* **547**, 79-83 (2017).

8. Gao, D.-W. et al. Cascade CuH-catalysed conversion of alkynes into enantioenriched 1,1-disubstituted products. *Nat. Catal.* **3**, 23-29 (2020).

9. Romano, C. & Martin, R. Ni-catalysed remote C(sp^3)–H functionalization using chain-walking strategies. *Nat. Rev. Chem.* **8**, 833-850 (2024).

10. Zhang, W. & Lin, S. Electroreductive carbofunctionalization of alkenes with alkyl bromides via a radical-polar crossover mechanism. *J. Am. Chem. Soc.* **142**, 20661-20670 (2020).

11. Li, Y. et al. Enantioselective alkene hydroalkylation overcoming heteroatom constraints via cobalt catalysis. *Nat. Synth.* **3**, 1134-1144 (2024).

12. Wang, Z., Yin, H. & Fu. G. C. Catalytic enantioconvergent coupling of secondary and tertiary electrophiles with olefins. *Nature* **563**, 379-383 (2018).

13. Seath, C. P., Vogt, D. B., Xu, Z., Boyington, A. J. & Jui, N. T. Radical hydroarylation of functionalized olefins and mechanistic investigation of photocatalytic pyridyl radical reactions. *J. Am. Chem. Soc.* **140**, 15525-15534 (2018).

14. Su, Y.-L. et al. Radical-mediated strategies for the functionalization of alkenes with diazo compounds. *J. Am. Chem. Soc.* **142**, 13846-13855 (2020).

15. Wheatley, E., Melnychenko, H. & Silvi, M. Iterative one-carbon homologation of unmodified carboxylic acids. *J. Am. Chem. Soc.* **146**, 34285-34291 (2024).

16. Bian, K.-J. et al. Photocatalytic hydrofluoroalkylation of alkenes with carboxylic acids. *Nat. Chem.* **15**, 1683-1692 (2023).

17. Zhu, Q. & Nocera, D. G. Photocatalytic Hydromethylation and Hydroalkylation of Olefins Enabled by Titanium Dioxide Mediated Decarboxylation. *J. Am. Chem. Soc.* **142**, 17913-17918 (2020).

18. Yang, T. et al. Chemoselective union of olefins, organohalides, and redox-active esters enables regioselective alkene dialkylation. *J. Am. Chem. Soc.* **142**, 21410-21419 (2020).

19. Chowdhury, R. et al. Decarboxylative alkyl coupling promoted by NADH and blue light. *J. Am. Chem. Soc.* **142**, 20143-20151 (2020).

20. Wang, J.-X., Fu, M.-C., Yan, L.-Y., Lu, X. & Fu, Y. Photoinduced triphenylphosphine and iodide salt promoted reductive decarboxylative coupling. *Adv. Aci.* **11**, 2307241 (2024).

21. Zhou, Z. et al. Direct stereoselective C(sp^3)–H alkylation of saturated heterocycles using olefins. *Nat. Chem.* **17**, 344-355 (2025).

22. Zhang, Z. et al. Enantioselective propargylic amination and related tandem sequences to α-tertiary ethynylamines and azacycles. *Nat. Chem.* **16**, 521-532 (2024).

23. Xu, P., Zhou, F., Zhu, L. & Zhou, J. Catalytic desymmetrization reactions to synthesize all-carbon quaternary stereocentres. *Nat. Synth.* **2**, 1020-1036 (2023).

24. Kar, S., Sanderson, H., Roy, K., Benfenati, E. &. Leszczynski, J. Green chemistry in the synthesis of pharmaceuticals. *Chem. Rev.* **122**, 3637-3710 (2022).

25. Yi, H. et al. Recent advances in radical C–H activation/radical cross-coupling. *Chem.*

412 *Rev.* **117**, 9016-9085 (2017).

413 26. Rivas, M., Palchykov, V., Jia, X. & Gevorgyan, V. Recent advances in visible light-
414 induced C(sp^3)–N bond formation. *Nat. Rev. Chem.* **6**, 544-561 (2022).

415 27. Biegasiewicz, K. F. et al. Photoexcitation of flavoenzymes enables a stereoselective
416 radical cyclization. *Science* **364**, 1166-1169 (2019).

417 28. Page, C. G. et al. Quaternary charge-transfer complex enables photoenzymatic
418 intermolecular hydroalkylation of olefins. *J. Am. Chem. Soc.* **143**, 97-102 (2021).

419 29. Huang, X. et al. Photoenzymatic enantioselective intermolecular radical
420 hydroalkylation. *Nature* **584**, 69-74 (2020).

421 30. Li, M., Harrison, W., Zhang, Z., Yuan, Y. & Zhao, H. Remote stereocontrol with
422 azaarenes via enzymatic hydrogen atom transfer. *Nat. Chem.* **16**, 277-284 (2024).

423 31. Li, M., Yuan, Y., Harrison, W., Zhang, Z. & Zhao, H. Asymmetric photoenzymatic
424 incorporation of fluorinated motifs into olefins. *Science* **385**, 416-421 (2024).

425 32. Bender, S. G. & Hyster, T. K. Pyridylmethyl radicals for enantioselective alkene
426 hydroalkylation using "ene"-reductases. *ACS Catal.* **13**, 14680-14684 (2023).

427 33. Huang, X. et al. Photoinduced chemomimetic biocatalysis for enantioselective
428 intermolecular radical conjugate addition. *Nat. Catal.* **5**, 586-593 (2022).

429 34. Duan, X. et al. A photoenzymatic strategy for radical-mediated stereoselective
430 hydroalkylation with diazo compounds. *Angew. Chem. Int. Ed. Engl.* **63**, e202214135
431 (2023).

432 35. Sun, S.-Z. et al. Enantioselective decarboxylative alkylation using synergistic
433 photoenzymatic catalysis. *Nat. Catal.* **7**, 35-42 (2024).

36. Yu, J. et al. Repurposing visible-light-excited ene-reductases for diastereo-and enantioselective lactones synthesis. *Angew. Chem. Int. Ed. Engl.* **63**, e202402673 (2024).

37. Zhao, B. et al. Direct visible-light-excited flavoproteins for redox-neutral asymmetric radical hydroarylation. *Nat. Catal.* **6**, 996-1004 (2023).

38. Jiang, L. et al. Photoenzymatic redox-neutral radical hydrosulfonylation initiated by FMN. *ACS Catal.* **14**, 6710-6716 (2024).

39. Shi, Q. et al. Single-electron oxidation-initiated enantioselective hydrosulfonylation of olefins enabled by photoenzymatic catalysis. *J. Am. Chem. Soc.* **146**, 2748-2756 (2024).

40. Liang, Y.-F. et al. Carbon–carbon bond cleavage for late-stage functionalization. *Chem. Rev.* **123**, 12313-12370 (2023).

41. O'Brien, T. E., Morris, A. O., Villela, L. F. & Barriault, L. Synthetic applications of photochemically generated radicals from protic C(sp^3)–H bonds. *ChemCatChem* **15**, e202300989 (2023).

42. Dong, M-Y. et al. Hydrogen-evolution allylic C(sp^3)–H alkylation with protic C(sp^3)–H bonds via triplet synergistic Brønsted base/Cobalt/photoredox catalysis. *ACS Catal.* **12**, 9533-9539 (2022).

43. Bas, S., Yamashita, Y. & Kobayashi, S. Development of brønsted base-photocatalyst hybrid systems for highly efficient C–C bond formation reactions of malonates with styrenes. *ACS Catal.* **10**, 10546-10550 (2020).

44. Palomo, C., Oiarbide, M. & Garcia, J. M. Current progress in the asymmetric aldol

addition reaction. *Chem. Soc. Rev.* **33**, 65-75 (2004).

45. Schetter, B. & Mahrwald, R. Modern aldol methods for the total synthesis of polyketides. *Angew. Chem. Int. Ed. Engl.* **45**, 7506-7525 (2006).

46. Tian, J. & Zhou, L. Photoredox radical/polar crossover enables C–H gem-difunctionalization of 1,3-benzodioxoles for the synthesis of monofluorocyclohexenes. *Chem. Sci.* **14**, 6045-6051 (2023).

47. Pitzer, L., Schwarz, J. L. & Glorius, F. Reductive radical-polar crossover: traditional electrophiles in modern radical reactions. *Chem. Sci.* **10**, 8285-8291 (2019).

Acknowledgements

This work was supported by the National Key R&D Program of China (2022YFA0912000), the Center of Synthetic Biology and Integrated Bioengineering (WU2022A006, WU2022A007, WU2023A009), the Research Center for Industries of the Future (WU2022C032). We thank Instrumentation and Service Center for Molecular Sciences (ISCMS) at Westlake University for the assistance in measurement and data interpretation. We thank Dr. Yinjuan Chen for the assistance with high resolution mass spectrometry (HRMS), Dr. Yuan Chen for the assistance with circular dichroism (CD), and Danyu Gu for the assistance with electron paramagnetic resonance (EPR).

Author contributions

J.Z. and Y.W. conceived and designed the overall project. J.Z. performed all synthetic

experiments and wet mechanism experiments. T.G., X.L., and M.-Z.M. created mutations. Q.Z., and X.W. carried out the computational studies and the calculation of absolute configuration (ECD) under the supervision of B.W. B.C. completed the calculation of redox potentials and Gibbs reaction energy (ΔG) for SET of Int. A. M.-J.M. performed the purification of some GluER variants. J.Z., B.W., and Y.W. wrote the paper with input of all authors.

Competing interests

The authors declare no competing interests.